10th International Conference on Control Engineering &Information Technology (CEIT-2025)
Proceedings Book Series –PBS- Vol 23, pp.187-202

Investigation of Impact of the DNG 2D Metamaterials on Refractive Indices

Marai M. Abousetta [*1], Abdussalam M. Ammar[*2]

[*1,2] *Microwave and Communication Engineering*, [*1,2] *Libyan Academy for Graduate Studies*

Tripoli – Libya

[1] m.abousetta@academy.edu.ly

[2]slm2010ly@gmail.com

Abstract— **In this study, we investigate the impact of double-negative (DNG) two-dimensional (2D) metamaterials on refractive indices using Plane Wave Expansion (PWE) and Finite-Difference Time-Domain (FDTD) methods. These metamaterials, characterized by simultaneous negative permittivity and permeability, exhibit unique electromagnetic properties, including negative refraction, reverse Doppler effect, and backward wave propagation. The PWE method is employed to compute the photonic band structure, revealing passband frequencies and bandgaps. The FDTD method, in contrast, provides a time-domain simulation of wave propagation, capturing the electromagnetic response via Fourier analysis. A comparative analysis of both methods confirms that DNG metamaterials effectively control wave propagation, with bandgaps restricting certain frequency components and passbands permitting transmission. These findings validate the feasibility of DNG metamaterials in waveguide applications, optical filtering, and electromagnetic shielding technologies.**

Keywords— **DNG , DPS ,EBG, HCG ,TE,TM .**

I. INTRODUCTION

In recent years, left-handed metamaterials (LHM) with their unique and new physical characteristics made these structures more appealing and interesting. The response of any material to the electromagnetic (EM) wave is mainly determined by two important parameters, dielectric permittivity (ε) and magnetic permeability (μ). In general ε and μ are known to be both positive in ordinary materials. But recent studies showed that for certain artificial structures, however, both the effective permittivity (ε_{eff}) and effective permeability (μ_{eff}) can have negative values.

The term "left-handed material" is used to describe such media because their electric, magnetic, and wave vector components combine to generate a left-handed (LH) coordinate system. The direction of the propagation is inverted relative to the direction of energy flow because the phase and group velocities are directed in opposing directions. In 1968, Veselago suggested that such an unusual material may exist if the dielectric permittivity and magnetic permeability were both less than zero. In his groundbreaking research, he also examined several optical characteristics for negative refractive index materials, including Doppler shift and Cherenkov radiation [1].

The idea of band structures in semiconductors was developed from the theory of electronic transport under periodic potentials. The wavefunctions needed to solve the Schrödinger equation are known as Bloch functions, named for the Swiss scientist Felix Bloch, who developed the quantum theory of solids in 1928 for his thesis, which are the product of $exp^{(ik\cdot r)}$ by periodic functions, k being the Bloch wavevector. Bands are obtained by computing the energy (or frequency) $\omega(k)$ and the eigenvectors (or quasinormal modes). In photonics, this solid-state approach is well described in ref. (Joan nopoulos et al., 2008), for instance [2].

In recent years, composite materials with concurrently negative permittivity and permeability values are attracting a lot of attention [3, 4, 5, 7]. The first system with these characteristics utilized an array of split-ring

ISSN: 2961-6611

resonators to produce negative permeability with an array of metallic wires to create negative permittivity [6]. The structure was used to illustrate negative refraction and showed backward-wave (BW) propagation characteristics. A new class of artificial electromagnetic materials, known as metamaterials, with unusual characteristics has emerged because of their use.

The potential subwavelength resolving capabilities of these materials [4] have sparked a lot of optimism and revived interest in electromagnetic phenomena related to materials having a negative refractive index (NRI) [6]. More recently, it was also demonstrated that an L-C loaded transmission line (TL) network deployed in cellular form had NRI features. The unit cell of the two-dimensional (2-D) NRI TL structure, which is utilized to experimentally illustrate negative refraction and focusing on microwave frequencies, is shown in Fig. 1 [7], [8].

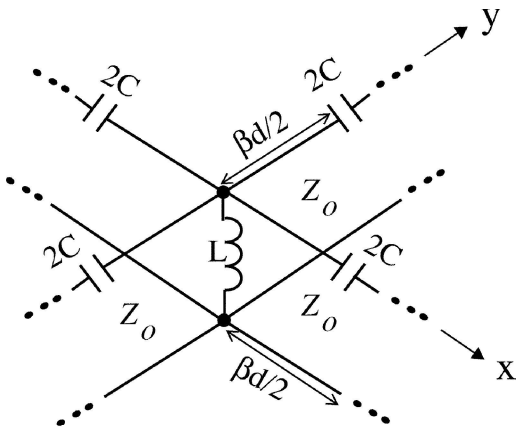

Fig. 1. The unit cell of a 2-D negative refractive index TL structure

II. THEORY OF PERIODIC STRUCTURE.

Phased arrays, electromagnetic bandgap (EBG) structures, frequency selective surfaces (FSS), and reflect arrays are only a few of the numerous practical uses for periodic structures in electromagnetics [9][10]. They have special qualities that may be utilized to improve electromagnetic absorption, electromagnetic propagation, and antenna gain. Repeating components in antenna arrays increase the effective aperture, which boosts the antenna's directivity and allows it to scan the main beam's direction if the right phase distribution is used. A periodic array of three-dimensional (3D) pillars, such as columns, cones, or prisms, has the potential to improve electromagnetic absorption in addition to planar elemental structures. This might improve performance in applications like microwave absorbers and solar cell efficiency [11]. Furthermore, new methods and analyses with suitable applications might be explored in the ongoing study of periodic structures.

A) One-Dimensional Photonic Crystals.

A multilayer thin film or Bragg's mirror might be used to describe the one-dimensional photonic crystal. Lord Rayleigh demonstrated the specifics of the multilayer thin film's optical properties in 1917 [12]. As seen in Fig. 2 where the different colors represent the contrast of the dielectric constants for each layer, the one-dimensional photonic crystal is made up of layers with varying dielectric constants layered on top of one another.

ISSN: 2961-6611

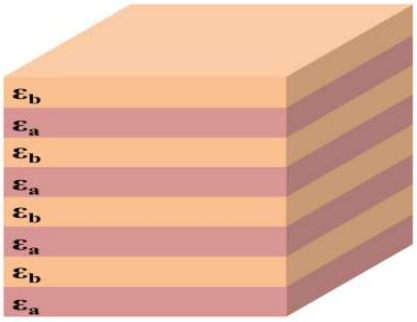

Fig 2. Multilayer thin film or one-dimensional photonic crystal.

The photonic bandgap forms in a single direction in a one-dimensional photonic crystal. Fig. 3 shows the plot of the band structure for the homogeneous one-dimensional photonic crystal in part (a) and the inhomogeneous one-dimensional photonic crystal in part (b), which was generated using the plane wave expansion (PWE) method. As seen in Fig. (1-3a), the isotropic one-dimensional photonic crystal is made up of layers with the same dielectric constant and has no photonic band gaps. The difference in the dielectric constants of the materials that made up the photonic crystals caused the photonic bandgaps to arise. The anisotropic one-dimensional photonic crystal's inset of Fig. (1-3b) makes this distinction evident [13,14].

B) Two-Dimensional Photonic Crystals.

The two-dimensional photonic crystal is homogeneous along the third axis and periodic along the other two. The propagation of the electromagnetic wave may be in the direction of x, y, and xy plane, but no propagation in the z direction. The photonic bandgap forms in the xy plane at specific values of the column spacing, a. A variety of electromagnetic wave frequencies are blocked from passing through the structure inside this photonic band gap, and incident light cannot pass through [13,14]. The two-dimensional photonic crystal can be represented as dielectric rods in air medium, as in part (a), or as a dielectric slab drilled with air cavities, as in part (b), as illustrated in Fig.4. However, as seen in both sections (a) and (b) of Fig. 4, the configuration of two-dimensional photonic crystals may be in the form of a square or hexagonal lattice.

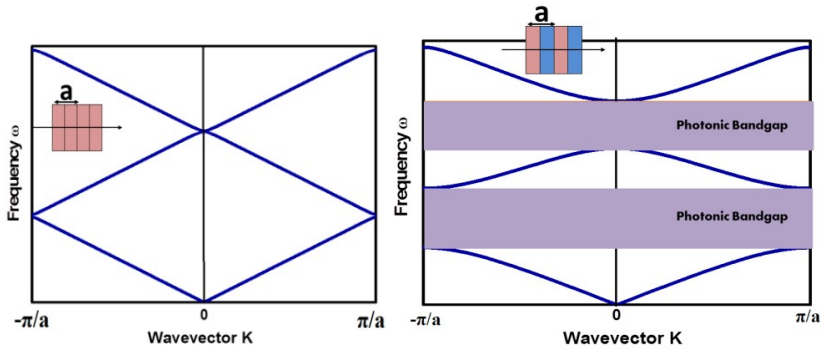

Fig 3. Band structure (dispersion relation) of (a) isotropic and (b) anisotropic one-dimensional photonic crystal.

ISSN: 2961-6611

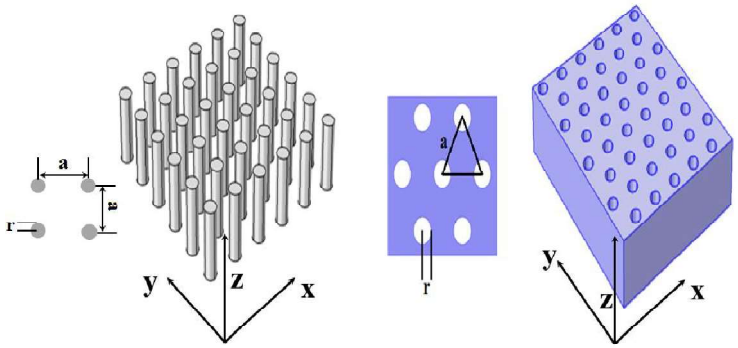

(a) (b)

Fig .4 Two-dimensional photonic crystals: (a) dielectric columns in an air medium and (b) dielectric slab with drilled air cavities.

The fingerprint of two-dimensional photonic crystals is the band structure, often known as the dispersion relation. Presenting the photonic crystal's band structure is crucial for demonstrating and validating the photonic bandgap's appearance. As seen in portion (a) of Fig. 5, the photonic bandgap in a two-dimensional photonic crystal is referred to as the entire photonic bandgap when it manifests itself in all directions of electromagnetic wave propagation. A different kind of two-dimensional photonic crystal has a photonic bandgap that forms at specific frequencies of electromagnetic waves and in a specific direction. These bandgaps, which are shown in part (b) of Fig. 5, are known as partial bandgaps, and their appearance is determined by the geometrical parameters in two-dimensional photonic crystals as well as the dielectric constants of the material [14,15].

C) Three-Dimensional Photonic Crystal.

The dielectric structure of this kind of photonic crystal exhibits periodicity along three distinct axes. There is no limit to the number of conceivable three-dimensional geometrical formations. Defect modes and photonic bandgaps are also present in the three-dimensional photonic crystal. In this kind of photonic crystal, the electromagnetic wave is confined in all three dimensions.

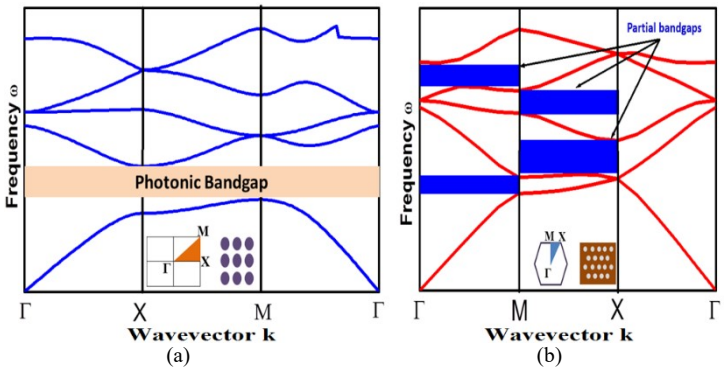

(a) (b)

Fig .5 Band structure of the two-dimensional photonic crystals showing: (a) Complete bandgap, and (b) Partial bandgaps..

So when we consider the one-dimensional photonic crystal (1D PhC), or equivalently, Bragg grating, refers to a layered structure that is periodic in one direction (chosen as x) and invariant in the other two directions ($y\ and\ z$), as shown in Fig. 6 (a). One-dimensional High Contrast Metastructure (HCM) [also known as a High Contrast Grating (HCG)] [16],[17] refers to alternating high-index (n_b) and low-index (n_a) media with a finite thickness t_g, as shown in Fig. 6(b).

ISSN: 2961-6611

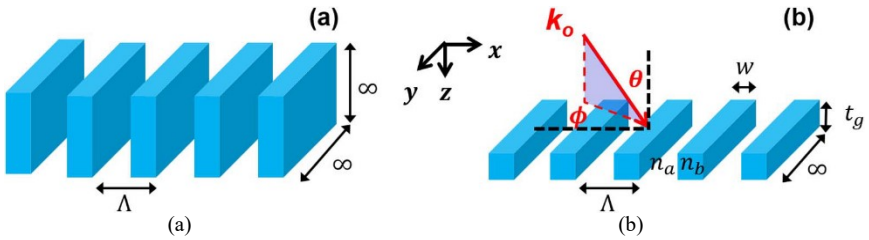

Fig.6. Schematics of (a) a 1D PhC and (b) a 1D high-contrast metastructure (also known as high-contrast gratings) with a finite thickness t_g.

Where period Λ, thickness t_g, bar width w, high-index material n_b for bars, and low-index material n_a for spaces between bars are examples of physical parameters. An incident plane wave has a wave number of k_0.

The incidence direction is defined by the polar angle θ and the azimuth angle ϕ. The incidence plane is the shaded plane in (b), defined by the surface-normal and the incidence directions. For 1D HCMs, x is the periodic direction and y is the invariant direction. For normal incidence ($\theta = 0$) on 1D HCMs, TE and TM are defined as the electric fields being parallel and perpendicular to the grating bars. For oblique incidence ($\theta \neq 0$), s polarization and p polarization refer to the electrical fields being perpendicular and parallel to the incidence plane, respectively.

III. Negative Refractive Index in Artificial Metamaterials.

We may create a new type of media categorization by using two electromagnetic constitutive parameters: the magnetic permeability μ and the electrical permittivity ε. Permittivity and permeability are frequently regarded as complex functions of the applied field's frequency as complex numbers enable the definition of magnitude and phase ,as follow [16] :

$$\varepsilon = \varepsilon' + \varepsilon'' \qquad (1)$$

Where ε' , $\varepsilon'' \in \Re$ and :

$$\mu = \mu' + \mu'' \qquad (2)$$

With $\mu', \mu'' \in \Re$

The Fig.7. shows this media classification in a diagram whose axis are formed by $\varepsilon' = \Re(\varepsilon)$ and $\mu' = \Re(\mu)$,

ISSN: 2961-6611

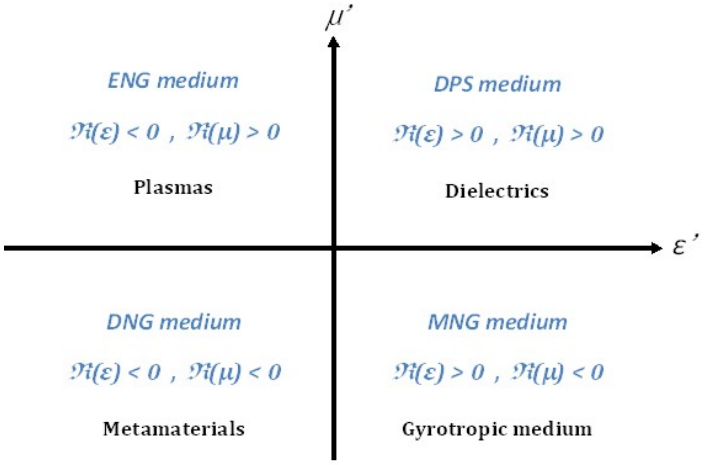

Fig 7. Material Classification by permittivity and permeability.

Considering that the electromagnetic wave is traveling along the z-axis and the electric field is polarized along the x-axis:

$$E = \hat{x}E_0 \exp\left[i(\mathbf{k}z - \omega t)\right] \qquad (3)$$

$$H = \hat{y}H_0 \exp\left[i(\mathbf{k}z - \omega t)\right] \qquad (4)$$

Where the complex wave number, k, is expressed as :

$$\mathbf{k} = k\hat{z} \qquad (5)$$

And the vacuum wave-number, k_0 ,is given by :-

$$k_0 = \omega\sqrt{\varepsilon_0\mu_0} = \frac{\omega}{c} \qquad (6)$$

where c is the speed of light and ω is the angular frequency.

From (5) and (6), it' s possible to write the refraction index, as function of frequency [14] :

$$n = \sqrt{\varepsilon\mu} \qquad (7)$$

With :

$$\eta = \frac{k}{\omega\varepsilon_0\varepsilon} = \frac{\omega\mu_0\mu}{k} = \zeta\eta_0 \qquad (8)$$

Leading us to :

$$\zeta = \frac{\eta}{\eta_0} = \sqrt{\frac{\mu}{\varepsilon}} \quad \text{where} \quad \eta_0 = \sqrt{\frac{\mu_0}{\varepsilon_0}} \qquad (9)$$

With η_0 being the vacuum wave impedance. Note that the normalized wave impedance can be re-written to:

$$\zeta = \frac{n}{\varepsilon} = \frac{\mu}{n} \qquad (10).$$

We must define a complex refraction index, since the polarization does not respond instantaneously to an applied field:

$$n = n' + in'' \qquad (11).$$

ISSN: 2961-6611

where n'' is the extinction coefficient and n' is the refractive index, which indicates the phase velocity coefficient. The amount of absorption loss that occurs when an electromagnetic wave passes through a material is indicated by the extinction coefficient. The frequency affects both n' and n'' [18].

Re-writing the complex amplitude equations for both the electric and the magnetic field using (11), we get:

$$E = \hat{x}E_0 \exp(-n''k_0 z)\exp(in'k_0 z) \qquad (12)$$

$$H = \hat{y}\frac{E_0}{\zeta\eta_0}\exp(-n''k_0 z)\exp(in'k_0 z) \qquad (13)$$

As we are dealing with the wave propagations in these materials, we need to consider the followings factors:

1) Backward Waves.

The left-hand rule may be readily absorbed from Maxwell's equations in the differential form as follow:

$$\nabla \times \mathbf{E} = -\frac{\partial \mathbf{B}}{\partial t} \qquad (14)$$

$$\nabla \times \mathbf{H} = -\frac{\partial \mathbf{D}}{\partial t} \qquad (15)$$

Also to describe the response of the medium to the applied fields, we have the following two constitutive relations,

$$\mathbf{B} = \mu_0\mu\mathbf{H} \quad , \quad \mathbf{D} = \varepsilon_0\varepsilon\mathbf{E} \qquad (16)$$

The relations between operators, in the time harmonic regime, can be derived:

$$\frac{\partial}{\partial t} \to -i\omega \quad , \quad \nabla \to i\mathrm{k} \qquad (17)$$

Using the following relations for the unique orientation of the electric and magnetic field vectors, **E** and **H**, we can determine the sign of the Poynting vector, S, and the wave vector, k:

$$\mathrm{k} \times \mathbf{E} = \omega\mu_0\mu\mathbf{H} \qquad (18)$$

$$\mathrm{k} \times \mathbf{H} = -\omega\varepsilon_0\varepsilon\mathbf{E} \qquad (19)$$

The electromagnetic wave and electromagnetic energy have the same direction in the DPS medium because both vectors, k and S, have the same direction, forming a forward wave as showing in Fig. 8. Additionally, in the DNG medium, the vectors k and S are oriented in the opposite directions. As a result, the electromagnetic wave and electromagnetic energy have opposing orientations, resulting in a reverse wave.

Based on (11) and (5), we can define the phase velocity, v_p, of an electromagnetic wave as following:

$$V_p = \frac{\omega}{\Re(\mathrm{k})} = \frac{\omega}{k_0\Re(\mathrm{n})} = \frac{c}{n\prime} \qquad (20).$$

ISSN: 2961-6611

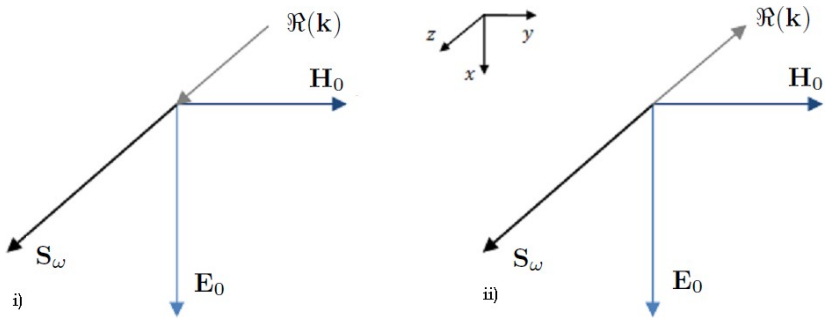

(a) (b)

Fig. 8. Trihedral vectors for the a) DPS and b) DNG media.

2) Dispersion.

From the laws of Electromagnetism, we know that for a certain isotropic medium, defined by ε and μ ,

$$\langle W_e \rangle = \frac{1}{4}\varepsilon\varepsilon_0 \bar{\mathrm{E}}.\bar{\mathrm{E}}^* \qquad (20)$$

$$\langle W_m \rangle = \frac{1}{4}\mu\mu_0 \bar{\mathrm{H}}.\bar{\mathrm{H}}^* \qquad (21)$$

In this case, the time-average magnetic density is $\langle W_m \rangle$ and the time-average electric density is $\langle W_e \rangle$. Since we cannot have a negative energy density, we face serious issues if both ε and μ are negative, as in DNG media. This demonstrates how the concept of electromagnetic energy requires a DNG medium to be dispersive. Therefore, both equations, (20) and (21), are invalid and need to be corrected to a lossless dispersive media [19] as follow:-

$$\langle W_e \rangle = \int_{-\infty}^{t} \frac{\partial \mathbf{D}}{\partial t'} \mathbf{E}\, dt' \qquad (22)$$

$$\langle W_m \rangle = \int_{-\infty}^{t} \frac{\partial \mathbf{B}}{\partial t'} \mathbf{H}\, dt' \qquad (23)$$

Both the electric and the magnetic fields are almost monochromatic, with $\mathrm{E(t)} = \bar{\mathbf{E}} \exp(-vt)$ and $\mathbf{H(t)} = \bar{\mathbf{H}} \exp(-vt)$ respectively, where the period variation is very slow $T = 2\pi/\omega$ meaning that $v \ll \omega$.

3) Group Velocity and Phase Velocity.

The expression for the time-average energy density of a monochromatic plane wave is defined by:

$$\langle W \rangle = \frac{1}{4}\left[\varepsilon_0 \frac{\partial(\omega\varepsilon)}{\partial\omega}|\mathbf{E}|^2 + \mu_0 \frac{\partial(\omega\mu)}{\partial\omega}|\mathbf{B}|^2\right] \qquad (24)$$

If we consider that :

$$A = \mu\varepsilon + \omega\mu\frac{\partial(\omega\varepsilon)}{\partial\omega} + \mu\varepsilon + \omega\varepsilon\frac{\partial(\omega\mu)}{\partial\omega} = 2\mu\varepsilon + \omega\left[\mu\frac{\partial(\omega\varepsilon)}{\partial\omega} + \varepsilon\frac{\partial(\omega\mu)}{\partial\omega}\right]$$

As seen in the previous section, in a DNG medium we have $\varepsilon < 0$ and $\mu < 0$, leading us to A < 0. From (10) we have,

$$\mathbf{k}^2 = \omega^2\mu_0\mu\varepsilon_0\varepsilon \qquad (25)$$

ISSN: 2961-6611

Applying the first derivative in order of the ω to $\mathbf{k}^2$, we get

$$\frac{\partial(\mathbf{k}^2)}{\partial\omega} = \mu_0\varepsilon_0\omega\left[2\varepsilon\mu + \omega\mu\frac{\partial(\omega\varepsilon)}{\partial\omega} + \omega\varepsilon\frac{\partial(\omega\mu)}{\partial\omega}\right] = \mu_0\varepsilon_0\omega A \quad (26)$$

Which gives the possibility to rewrite Equ. (26) as follow :

$$\frac{\partial(\mathbf{k}^2)}{\partial\omega} = 2\mathbf{k}\frac{\partial(\mathbf{k})}{\partial\omega} = 2nk_0\frac{\partial(\mathbf{k})}{\partial\omega} = 2\mathbf{n}\frac{\omega}{c}\frac{\partial(\mathbf{k})}{\partial\omega} \quad (27)$$

The Phase Velocity, $\mathbf{v}_p$, is given by:

$$\mathrm{v}_p = \frac{\omega}{\Re(\mathrm{k})} = \frac{\omega}{k_0\Re(\mathrm{n})} = \frac{c}{\mathrm{n}\prime} \quad (28)$$

and the Group Velocity, $\mathbf{v}_g$, is given by:

$$\mathbf{v}_g = \frac{\partial\omega}{\partial\mathrm{k}} \quad (29)$$

For a lossy DNG medium, ε< 0 and μ< 0, we have $\mathcal{A}$< 0 which implies that

$$\frac{\partial(\mathrm{k}^2)}{\partial\omega} < 0 \quad (30)$$

Since we cannot have negative energy density, we must conclude that v_g and $\mathbf{v}_p$ have different signs (and opposite directions). For a non-dispersive media, one has $\mathbf{v}_g$ = $\mathbf{v}_p$. On the DNG media, that must be dispersive, one can prove that both group velocity and phase velocity, not only have different signs, but also has different values.

From (28) and (29) we get :

$$\frac{1}{\mathbf{v}_g} = \frac{1}{\mathbf{v}_p} + \frac{1}{c}\omega\frac{\partial n}{\partial\omega} \quad (31)$$

Due to last parcel, the group velocity is only equal to the phase velocity when the refraction index is frequency independent.

4) Most used Metamaterial Types with Refractive Indices.

As part of this search we list some of commonly used metamaterials and their refractive indices, which are typically tailored to specific frequency ranges (e.g., microwave, terahertz, infrared, optical).

i- Split-Ring Resonators (SRRs): Composed of metallic rings with splits, these are widely used to achieve negative permeability, and the refractive index could be negative in specific frequency ranges, typically around -1 to -5 in the microwave or terahertz regimes.
ii- Photonic Crystals (PhC): Periodic dielectric structures that manipulate light by creating photonic band gaps, and the refractive index typically ranges from 1.5 to 4, depending on the materials used.
iii- Metal-Dielectric Metamaterials: composed of Alternate layers of metals (e.g., silver, gold) and dielectrics (e.g., silica, titania), and refractive index can achieve values close to zero (epsilon-near-zero materials) or negative, depending on the design.
iv- Chiral Metamaterials: Asymmetric structures that exhibit chirality, allowing for circular dichroism and polarization rotation, refractive index can have negative refractive indices (typically -1 to -3) for circularly polarized waves.
v- Terahertz Metamaterials: Designed to operate in the terahertz frequency range, typically combining metallic and dielectric components, refractive index tuneable between positive and negative values, depending on the design.
vi- Plasmonic Metamaterials: Exploits surface plasmon resonances at the interface of metals and dielectrics, with negative refractive indices around -1 in the optical regime.

ISSN: 2961-6611

vii- Double-Negative (DNG) Metamaterials: Exhibit both negative permittivity ($\varepsilon < 0$) and permeability ($\mu < 0$), for refractive index will be highly negative, typically ranging from -1 to -10.

IV. Analytical and Numerical Methods for Periodic Structures.

Modeling periodic structures requires considering the dispersion of modes, photonic band structures, resonances and quality factors, the total field distribution, and the complicated reflection and transmission coefficients of diffraction orders. Table (1) compares the calculation methodology of the six main analytical and numerical modeling approaches for periodic structures.

The three primary methods in computational electromagnetics (CEM) are the method of moments (MoM) [20], the finite-element method (FEM) [20,21], and the finite-difference time-domain (FDTD) [40,41]. MoM is an integral equation solver that is generated using Green's function, whereas FDTD and FEM are differential equation solvers that discretize either the differential operator or the solution. The convergence rate and computing cost for big problems have long been difficulties since FDTD and FEM discretize the whole solution domain.

Table (1). Comparison among Various Computation Methods for Periodic Structures

Method	How to solve?	What to be solved	Results
Finite-difference time-domain (FDTD)	1-Discretize differential operator into matrix. 2- Expand fields with delta functions $\delta(x_i; y_i; z_i)$ on finite difference grids $(x_i; y_i; z_i)$. 3- Build matrix equation and solve in time domain	Fields on grids E$(x_i; y_i; z_i)$ And H $(x_i; y_i; z_i)$	Total fields $\boldsymbol{E}(\boldsymbol{r}), \boldsymbol{H}(\boldsymbol{r})$
Finite element method (FEM)	1-Expand fields in frequency domain with basis functions $\boldsymbol{\psi_i}(\boldsymbol{r})$, predefined commonly on elements in triangular or tetrahedral meshes. 2-Build matrix equation from basis functions.	Expansion coefficients $\boldsymbol{a_i}$	Total fields $\boldsymbol{E}(\boldsymbol{r}), \boldsymbol{H}(\boldsymbol{r})$
Method of moments (MoM)	1-Express fields in integral equations based on known Green's functions $\bar{\boldsymbol{G}}(\boldsymbol{r}, \boldsymbol{r}')$. 2-Expand surface currents and build matrix equations.	Surface electric and magnetic currents $\boldsymbol{J}(\boldsymbol{r}'), \boldsymbol{M}(\boldsymbol{r}')$	Scattered fields $\boldsymbol{E_s}(\boldsymbol{r}), \boldsymbol{H_s}(\boldsymbol{r})$
Rigorous coupled wave Analysis (RCWA)	1-Predefine Bloch waves in each layer $\boldsymbol{e^{iG_x x+G_y y}}$. 2- Solve eigenmodes in each layer $\varepsilon^{(i)}, \boldsymbol{\mathcal{H}}^{(i)}(\boldsymbol{r})$. 3- Find propagation matrices and interface transfer matrices	1- Expansion coefficients in each layer $\widetilde{\boldsymbol{E}}_{\boldsymbol{G}}$, $\widetilde{\boldsymbol{H}}_{\boldsymbol{G}}$ to build $\boldsymbol{ith}$ eigenmodes in Eq.$\varepsilon^{(i)}(\boldsymbol{r}) = \sum_G \widetilde{\boldsymbol{E}}_{\boldsymbol{G}} \boldsymbol{e^{iG.r}}$. 2- Eigenmodes coefficients $\boldsymbol{A_i}$ to build supermodes in Eq:$\boldsymbol{E}(\boldsymbol{r}) = \sum_i \boldsymbol{A_i} \varepsilon^{(i)}(\boldsymbol{r})$.	1-Eigenmodes in each layer. 2-Supermodes in each layer. 3-Total fields
Plane wave expansion (PWE)	1-Predefine Bloch waves in each layer $\boldsymbol{e^{iG.r}}$. 2-Cast wave equation into matrix equation and solve for expansion coefficients	Expansion coefficients $\widetilde{\boldsymbol{E}}_{\boldsymbol{G}}$, $\widetilde{\boldsymbol{H}}_{\boldsymbol{G}}$ to build eigenmodes in the entire domain $\boldsymbol{E}(\boldsymbol{r}) = \sum_G \widetilde{\boldsymbol{E}}_{\boldsymbol{G}} \boldsymbol{e^{iG.r}}$	Eigenmodes in the entire domain
Analytical mode-matching (AMM)	1-Predefine analytical Eigenmodes $\varepsilon^{(i)}(\boldsymbol{r}), \boldsymbol{\mathcal{H}}^{(i)}(\boldsymbol{r})$. 2-Find analytical interface matrices.	Eigenmode expansion coefficients $\boldsymbol{a_i}$ to build super-modes in each layer	1-Supermodes in each layer. 2-Total fields

Furthermore, it is relatively problematic for FDTD and FEM to separate and extract modes or diffraction orders from periodic structures since the solution is the complete field. MoM is effective for scattering issues because it can acquire fields across the space by computing just the fields at borders. Although the necessary

ISSN: 2961-6611

computation of the periodic Green's function has sluggish convergence, it may easily provide scattering coefficients for distinct diffraction orders [22].

Neither FDTD, FEM, nor MoM reveals the eigenmodes and their properties in the periodic region and, therefore, much of the underlying physics is hidden. RCWA and the plane-wave expansion (PWE) method are two widely used approaches for HCMs and PhCs, respectively. According to the Floquet–Bloch theorem the fields in periodic media can be expanded using the Bloch waves $e^{iG.r}$, as shown in Table (1). The expansion coefficients $\tilde{E}_G$, $\tilde{H}_G$ for these Bloch waves are the unknowns to solve. These are the ways that RCWA and PWE vary from one another. RCWA is popular in layered media with periodic structures because it solves the eigenmodes $\mathcal{E}^{(i)}(\boldsymbol{r})$, $\boldsymbol{\mathcal{H}}^{(i)}(\boldsymbol{r})$ layer by layer through the Bloch waves. PWE is widely utilized in the computation of PhC band structure and extends the full domain in Bloch waves. Each area, including the periodic layer, is first regarded as an infinitely long waveguide array in RCWA, and its eigenmodes are then determined.

As a result, we know which modes radiative waves may couple to or excite. Understanding their respective optical phases and propagation velocities is also helpful. In this manner, any unusual optical behavior may be achieved by engineering the interference at area contacts [23,24,25]. We acquire the interface transfer matrices and solve the eigenmode expansion coefficients once each layer interface's boundary conditions are matched. This allows us to understand how the eigenmodes in each layer create "super-modes," which are essential for designing and explaining the exceptional performance of HCMs, including ultrahigh-Q resonance and 100% reflection and transmission [23, 25]. However, because PWE solves individual eigenmodes throughout the whole domain, it does not have this information.

As indicated in Table 2, an alternative method is to first analytically express the eigenmodes in each region, which may then be utilized as the foundation for eigenmode expansion. Here, eigenmodes serve as the foundation for an array of complex expansion coefficients ai that may be used to represent fields in each layer. Known as the analytical technique or analytical mode-matching (AMM), this approach has been thoroughly covered in Refs. [23,25] and is proven to be very accurate and effective for creating 1D HCGs. As with RCWA, the resonance and coupling may be studied by obtaining the super-modes created by the eigenmodes in each layer.

The following is a comparison between the AMM and RCWA. In the case of 1D HCGs, the eigenmodes are analytically rigorous scalar sinusoidal functions. Consequently, only the finite number of eigenmodes used in the computation account for the numerical inaccuracy in AMM. By matching boundary conditions, transfer and scattering matrices are analytically constructed at the interfaces between periodic and homogeneous areas. Furthermore, it excels at exposing the fundamental physics, producing useful tools for clear designs [23, 25]. However, problems occur when the periodicity reaches 2D or when the grating cross section is not rectangular [24].

In these situations, there are no rigorous closed-form formulas for the vectorial eigenmodes. Both the calculation cost for numerical overlap integrals in the interface matrix elements and the memory cost for storing the mode profiles are high, even if the eigenmodes are solved numerically. To get over these issues, RCWA further projects these eigenmodes onto the Bloch basis, which is made up of exponential functions $e^{iG.r}$, as Table (1) illustrates. The complex vectors $\tilde{\mathbf{E}}_G^{(i)}$ and $\tilde{\mathbf{H}}_G^{(i)}$ are the expansion coefficients.

Eigenmodes are solved and represented in the Fourier domain in this instance with minimal memory and compute costs. However, the disadvantage of employing RCWA without determining the eigenmodes is that, because there is no physical interpretation to account for the modes, it is very challenging to distinguish resonances from numerical noise. This is especially true for high-Q resonator designs or when there are unusual dips in the broadband transmission or reflection spectra.

ISSN: 2961-6611

Table (2) lists the capabilities of the various modeling approaches in comparison. Here we outline the key findings. (i) Since PWE exclusively solves eigenmodes, all six methods aside from PWE can determine the total fields under stimulation. (ii) MoM, RCWA, and AMM can be used to solve the transmission and reflection of each diffraction order, but PWE cannot. For FDTD and FEM to distinguish the diffraction orders, the whole fields must be postprocessed. (iii) Using the scattering spectra in FEM, MOM, RCWA, and AMM, the resonance frequency ω_r is calculated and solved as the eigenfrequencies in PWE.

Table 2: Capabilities of Various Computation Methods for Periodic Structures

Method	Total field under Excitation	ω_r	Q	Band Structure	Eigenmode and Dispersion
FDTD	Cal	Cal	Cal	Cal	
FEM	Cal	Cal	Cal		Cal
MoM	Cal	Cal	Cal		
RCWA	Cal	Cal	Cal		Cal
PWE		Cal	Cal	Cal	Cal
Anal	Cal	Cal	Cal		Cal

Where “cal” indicates directly calculated or simple extraction.

The resonance frequency is also provided by the Fourier transform of the FDTD result. (iv) The spectral linewidth in FEM, MOM, RCWA, and AMM, as well as the temporal decay in FDTD, are used to derive the Q of a resonant mode. (v) It is difficult to extract the band structure from the scattering spectra obtained by FEM, MoM, RCWA, and AMM.

These scattering spectra, however, may be verified and compared to the band structure derived by PWE. In order to produce significant band structures with FDTD, it is crucial to carefully set up the excitation sources and observation sites. This will be covered in following sections. (vi) Eigenmodes and their dispersion cannot be provided by FDTD as a time-domain solution. The eigenmodes can be obtained by solving the eigenvalue problem with the excitation source suppressed using frequency-domain solvers such as FEM, RCWA, PWE, and AMM.

IV. Analysis of Simulation Results.

For this simulation it is proposed to use PWE and FDTD methods to figure out many properties of DNG metamaterials and the wave propagation through it such as negative refraction, reverse Doppler effect, and backward wave propagation. Both the PWE method and the FDTD method are commonly used to analyses and simulate these materials.

The analysis focuses on key aspects such as passbands, bandgaps, frequency response, and wave propagation characteristics. Where the PWE method successfully identifies passbands and bandgaps in the structure, and for The FDTD frequency response (FFT analysis of the time-domain signal) provides a direct representation of how the material responds to wave excitation as in Fig. 9.

ISSN: 2961-6611

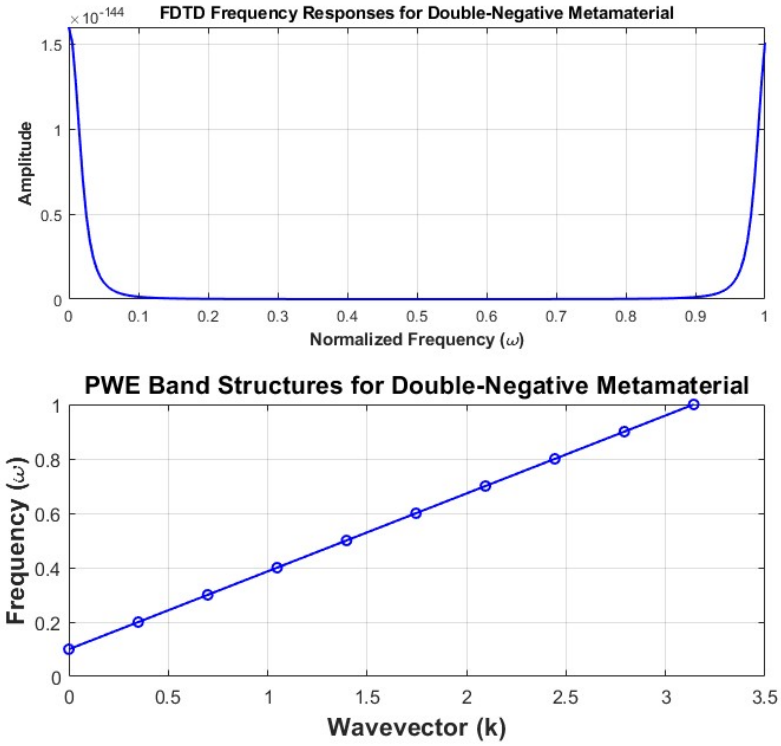

Fig. 9. The FDTD frequency response and PWE band structure for DNG metamaterials.

For PWE method the photonic band structure shows allowed propagation frequencies and forbidden frequency regions (bandgaps), and the band structure confirms that the double-negative metamaterial exhibits negative refractive index behaviour, supporting unusual propagation characteristics. The passband frequencies correspond to regions where wave propagation is allowed, also the bandgaps are regions where wave propagation is forbidden, meaning that any wave in these frequencies will be attenuated.

It is notable also that the presence of multiple bandgaps suggests that the structure strongly controls the propagation of electromagnetic waves, making it suitable for applications such as filters and waveguides. For FDTD results, the peaks in the FFT signal correspond to the dominant frequencies of propagation and the FDTD results confirm the passband frequencies obtained from PWE, validating the theoretical band structure, also the absence of significant peaks in bandgap regions confirms wave attenuation in those frequency ranges.

The FDTD results show that waves propagate only in the allowed passbands identified by PWE, the absence of response in bandgap regions suggests that the metamaterial effectively blocks certain frequency components, consistent with negative-index material behaviour. As the FFT signal shows peaks aligning with PWE passbands, indicating that the material permits electromagnetic wave transmission at these frequencies. In Fig.10. comparison between the PWE method and the FDTD method for analysing the electromagnetic response of a double-negative metamaterial (DNG), the red circles represent the PWE band structure, showing discrete frequency points where wave propagation is allowed, where is the blue line represents the FDTD response, which appears to align closely with the PWE results.

ISSN: 2961-6611

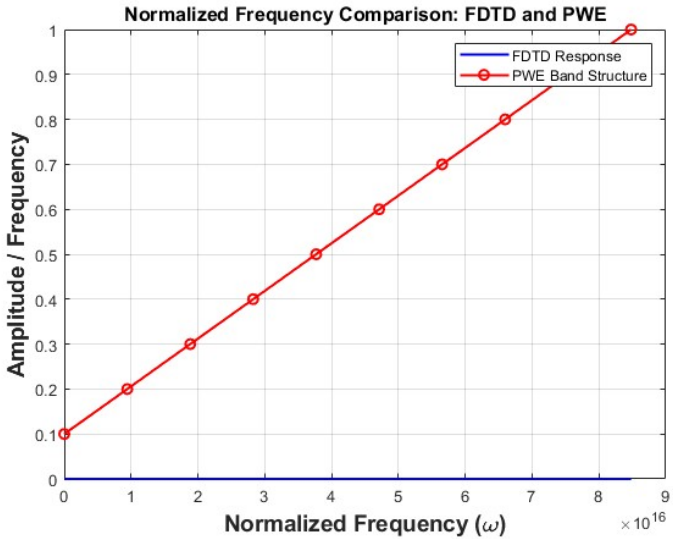

Fig.10. normalized frequency comparison between FDTD and PWE methods

In prospective of linear dispersion relationship, the nearly linear trend in the frequency response suggests a homogeneous medium-like behaviour. In double-negative metamaterials, wave dispersion behaves differently than in conventional materials, but the observed linearity here may be due to the selected wave vector range and frequency normalization. Also, notable that the blue FDTD response is almost zero at low frequencies, which suggests that wave propagation is restricted (due to bandgap). this behaviour aligns with the expected bandgap regions in DNG materials, where certain frequencies cannot propagate. The close match between PWE and FDTD results validates the computational model, confirming that both approaches predict the same band structure and propagation characteristics.

V. CONCLUSION

This research highlights the distinct wave manipulation capabilities of DNG metamaterials, demonstrated through both PWE and FDTD numerical techniques. The PWE band structure analysis confirms the presence of well-defined passbands and bandgaps, showcasing the ability of these materials to block or transmit specific electromagnetic frequencies. The FDTD simulation further validates this behavior, with frequency response peaks aligning with the PWE passbands, reinforcing the reliability of both computational approaches. A significant observation is the close agreement between theoretical and numerical results, proving that DNG metamaterials enable negative refraction and backward-wave propagation. The analysis also demonstrates that these structures can be engineered for photonic devices, waveguides, and cloaking technologies, where precise control over wave transmission and reflection is required.

Future work could extend this investigation by exploring 3D metamaterial structures, optimizing geometrical parameters to enhance bandwidth control, and applying these principles to microwave and optical communication systems. The potential of DNG metamaterials in next-generation photonic devices is vast, making them a promising area for continued research and development.

This document is a template. An electronic copy can be downloaded from the conference website. For questions on paper guidelines, please contact the conference publications committee as indicated on the conference website. Information about final paper submission is available from the conference website.

REFERENCES

[1] V. G. Veselago, “The electrodynamics of substances with simultaneously negative values of _ and _,” Sov. Phys. Usp., vol. 10, pp. 509–514, Jan.-Feb. 1968

[2] Joannopoulos, J. D., Johnson, S. G., Winn, J. N., and Meade, R. D.. “Photonic Crystals: Molding the Flow of Light. Princeton University Press, Princeton, (Second Edition), (2008).

ISSN: 2961-6611

[3] D. R. Smith, W. J. Padilla, D. C. Vier, S. C. Nemat-Nasser, and S. Schultz, “Composite medium with simultaneously negative permeability and permittivity,” Phys. Rev. Lett., vol. 84, pp. 4184–4187, May 2000.
[4] J. B. Pendry, “Negative refraction makes a perfect lens,” Phys. Rev. Lett., vol. 85, pp. 3966–3969, Oct. 2000.
[5] D. R. Smith and N. Kroll, “Negative refractive index in left-handed materials,” Phys. Rev. Lett., vol. 85, pp. 2933–2936, Oct 2000.
[6] R. A. Shelby, D. R. Smith, and S. Schultz, “Experimental verification of a negative index of refraction,” Science, vol. 292, pp. 77–79, Apr. 2001.
[7] A. K. Iyer and G. V. Eleftheriades, “Negative refractive index metamaterials supporting 2-D wave propagation,” IEEE MTT-S Int. Microwave Symp. Dig., vol. 2, pp. 1067–1070, June 2002.
[8] G. V. Eleftheriades, A. K. Iyer, and P. C. Kremer, “Planar negative refractive index media using periodically L-C loaded transmission lines,” IEEE Trans. Microwave Theory Tech., vol. 50, pp. 2702–2712, Dec. 2002.
[9] R. Haupt, Antenna Arrays: A Computational Approach. Englewood Cli s,New Jersey: Wiley, 2010.
[10] H. Rajagopalan, Y. Rahmat-Samii, and W. A. Imbriale, \Rf mems actuated reconfigurable reflect array patch-slot element," IEEE Transactions on Antennas and Propagation, vol. 56, pp. 3689{3699, December 2008.
[11] L. Hu and G. Chen, \Analysis of optical absorption in silicon nanowire arrays for photovoltaic applications," Nano Letters, vol. 7, p. 3249, 2007.
[12] L. Rayleigh, Proc. Royal Society of London, 565-577: 93, 1917.
[13] J. D. Joannopoulos, S.G. Johnson, J. N. Winn, R. D. Meade, Photonic Crystals Molding the Flow of Light, Princeton University Press, Princeton, New Jersey, 2007.
[14] B. E. A. Saleh , M. C. Teich, Fundamental of Photonics, 2nd edition, Wily Interscience, 1991.
[15] F. Shanhui, P. R. Villeneuve, and J. D. Joannopoulos, Journal of Applied Physics, 1415-1418: 78. 1995.
[16] C. F. R. Mateus, M. C. Y. Huang, C. Lu, C. J. Chang-Hasnain, and Y. Suzuki, “Broad-band mirror (1.12–1.62 μm) using a subwavelength grating,” IEEE Photon. Technol. Lett. 16, 1676–1678 (2004).
[17] C. J. Chang-Hasnain and W. Yang, “High-contrast gratings for integrated optoelectronics,” Adv. Opt. Photon. 4, 379–440 (2012).
[18] C. R. Paiva, Meios Duplamente Negativos (DNG), DEEC-IST,2008.
[19] L. Solymar, E. Shamonina, Waves in Metamaterials, Oxford University Press, 2009.
[20] W. C. Chew, E. Michielssen, J. M. Song, and J.-M. Jin, Fast and Efficient Algorithms in Computational Electromagnetics (Artech House, 2001).
[21] J.-M. Jin, The Finite Element Method in Electromagnetics (Wiley, 2015).
[22] R. E. Jorgenson and R. Mittra, “Efficient calculation of the free-space periodic Green’s function,” IEEE Trans. Antennas Propag. 38, 633–642 (1990).
[23] C. J. Chang-Hasnain and W. Yang, “High-contrast gratings for integrated optoelectronics,” Adv. Opt. Photon. 4, 379–440 (2012).
[24] P. Qiao, L. Zhu, W. C. Chew, and C. J. Chang-Hasnain, “Theory and design of two-dimensional high-contrast-grating phased arrays,” Opt. Express 23, 24508–24524 (2015).
[25] V. Karagodsky, F. G. Sedgwick, and C. J. Chang-Hasnain, “Theoretical analysis of subwavelength high contrast grating reflectors,” Opt. Express 18, 16973– 16988 (2010).

ISSN: 2961-6611